ChemistrySelect

Research Article
doi.org/10.1002/slct.202500457

Chemistry Europe
European Chemical Societies Publishing

www.chemistryselect.org

Co-Binding of Methotrexate and Cyclophosphamide via Folic Acid-Decorated Graphene Oxide Nanomaterials for Therapeutic Approach against Breast Cancer

Reyhan Yanıkoglu,*[a] Canan Yagmur Karakas,[b] Mert Akın Insel,[c] Merve Sevgi,[a] Esmahan Caglar,[a] Hasan Berkay Abdioğlu,[d] Yagmur Isık,[d] Hilal Calık,[a] Ali Can Zaman,[e] Fatih Ciftci,[f] Rabia Cakır,[a] Huseyin Uvet,[d] and Cem Bulent Ustundag[a, g]

In this study, we developed a graphene oxide (GO)-based nanocarrier system co-loaded with methotrexate (MTX) and cyclophosphamide (CP) and functionalized with folic acid (FA) for targeted drug delivery. The synthesized CP/MTX/FA/GO system and its individual components were characterized by zeta potential analysis, FTIR spectroscopy, FE-SEM imaging, and DSC analysis. Structural characterization revealed that the 3D morphology of the CP/MTX/FA/GO formulation was denser compared to CP/FA/GO and MTX/FA/GO systems. FTIR and DSC results confirmed the successful oxidation of graphite and the physicochemical incorporation of CP, MTX, and FA into the GO structure through functional groups such as carboxylic, hydroxyl, epoxide, and carbonyl. In vitro release studies using Franz diffusion demonstrated that the drug release profile followed the Higuchi model with a high correlation coefficient ($R^2 = 0.9837$), indicating that the release was primarily governed by Fickian diffusion, where drug transport occurs along a concentration gradient through the GO matrix. Stiffness analysis indicated that FA functionalization enhanced cell targeting and facilitated drug internalization. Cytotoxicity assays showed that CP/MTX/FA/GO exerted a significantly higher antiproliferative effect on MDA-MB-231 breast cancer cells compared to free MTX, free CP, CP/FA/GO, and MTX/FA/GO. Collectively, these findings suggest that the CP/MTX/FA/GO nanocarrier exhibits strong potential for dual-drug targeted therapy, offering synergistic cytotoxic effects and efficient drug delivery.

1. Introduction

Cancer continues to be the second leading cause of death worldwide, and its incidence has been steadily increasing.[1] In men, the most frequently diagnosed cancers include prostate, lung and bronchus, colorectal, and bladder cancers. Among women, breast, lung, colorectal, uterine, and thyroid cancers are the most prevalent. These statistics indicate that prostate cancer in men and breast cancer in women remain the most common types.[2]

While conventional therapies—especially chemotherapy—have long been the cornerstone of cancer treatment, they are not always sufficient to prevent mortality during or after the course of treatment.[3,4] This has led researchers to explore alternative approaches that may offer improved outcomes. In recent years, considerable attention has been directed toward emerging strategies such as gene therapy, stem cell-based interventions, natural antioxidants, photodynamic therapy, nanotechnology-enabled platforms, and precision medicine. Among these, targeted drug delivery systems have shown significant promise and form the basis of the current investigation.[3]

The periodic table's Group IVA contains carbon, which is the lightest element. Carbon nanomaterials, which come in a variety of allotropes, are the only substances that have been shown to exist steadily in all dimensions, including 1D carbon nanotubes, 2D graphene, 3D diamond, and graphite.[5] These car-

[a] R. Yanıkoglu, M. Sevgi, E. Caglar, H. Calık, R. Cakır, C. B. Ustundag
Department of Bioengineering, Faculty of Chemical and Metallurgical Engineering, Yıldız Technical University, Istanbul 34210, Türkiye
E-mail: reyhanyanikoglu@gmail.com

[b] C. Y. Karakas
Department of Food Engineering, Faculty of Chemical and Metallurgical Engineering, Yıldız Technical University, Istanbul 34210, Türkiye

[c] M. Akın Insel
Department of Chemical Engineering, Faculty of Chemical and Metallurgical Engineering, Yıldız Technical University, Istanbul 34210, Türkiye

[d] H. B. Abdioğlu, Y. Isık, H. Uvet
Department of Mechatronics Engineering, Faculty of Mechanical Engineering, Yıldız Technical University, Istanbul 34210, Türkiye

[e] A. C. Zaman
Department of Metallurgical and Materials Engineering, Faculty of Chemical and Metallurgical Engineering, Yıldız Technical University, Istanbul 34210, Türkiye

[f] F. Ciftci
Department of Biomedical Engineering, Fatih Sultan Mehmet Vakif University, Istanbul 34445, Türkiye

[g] C. B. Ustundag
Health Biotechnology Joint Research and Application Center of Excellence, Istanbul 34220, Türkiye

bon nanomaterials have attracted attention in recent years with their use in much research and many applications. Such studies include supercapacitors,[6] environmental applications,[7,8] tissue engineering,[9–11] electronic devices,[12] bio-imaging,[13] and sensors,[14] including drug delivery systems. Among these nanomaterials, graphene oxide (GO) stands out as a 2D sheet composed of a single atomic layer of sp^2-hybridized carbon atoms functionalized with oxygen-containing groups such as hydroxyl, carboxyl, and epoxy moieties.[15] This ultrathin, flexible structure not only enables a high surface area for drug loading but also facilitates chemical conjugation with various therapeutic agents.[16] Due to these unique physicochemical properties, GO has emerged as a promising nanoplatform for drug delivery applications, particularly in cancer therapy.[17,18] Although the lateral dimensions of GO-based carriers may exceed the conventional nanocarrier range of 10–1000 nm, their nanometer-scale thickness (typically 1–10 nm) allows them to retain critical nanoscale behavior in biological environments.[19]

Methotrexate (MTX), a WHO "essential medicine," was created more than 70 years ago as an anti-folate chemotherapeutic agent and is currently used extensively as a first-line treatment for inflammatory and autoimmune illnesses such as Crohn's disease, psoriasis, and rheumatoid arthritis (RA).[20] This medication is used to treat ectopic pregnancy as well as a number of malignant conditions, including leukemia and cancers of the breast, uterus, and lung.[21] There have been various studies on drug delivery systems for this drug in recent years.[22–24] Since the 1960s, cyclophosphamide (CP), an alkylating drug, has been used to treat severe symptoms of autoimmune inflammatory disease.[25] Many cancers, including multiple myeloma,[26] breast cancer,[27] and renal disorders, such as focal segmental glomerulonephritis and nephrotic syndrome unresponsive to corticosteroid,[28–30] are treated with cyclophosphamide. In recent years, scientists have been investigating the use of CP in drug delivery systems.[31,32] Vitamin B9, commonly known as folate, is a water-soluble vitamin present in a wide range of foods. It exists in two main forms: the oxidized synthetic form known as folic acid and the reduced, naturally occurring form referred to simply as folate.[33] FA, sometimes referred to as vitamin B9, has been studied for its potential in targeted delivery of drugs, especially in the context of cancer therapy.[34,35] Targeted delivery of therapeutic drugs using specific cellular markers can enhance efficacy while minimizing off-target toxicity. The folate receptor (FR), which exists in two isoforms—FR-α and FR-β—is anchored to the cell membrane via a glycosylphosphatidylinositol (GPI) linkage. Folate receptor-targeted therapies have shown promising results in preclinical models and hold considerable potential for future clinical applications across a wide range of diseases.[36,37]

The nanosystem developed in this study serves two primary purposes: (i) to enable targeted delivery of chemotherapeutic agents—methotrexate (MTX) and cyclophosphamide (CP)—to cancer cells by co-loading them onto a graphene oxide (GO) carrier functionalized with folic acid (FA), and (ii) to enhance therapeutic efficacy through the synergistic interaction of the two drugs. This strategy is intended to maximize drug effectiveness while minimizing adverse effects on healthy tissues, potentially reducing side effects and lowering required dosages. A recent study by Yanikoglu et al.[18] reported the development of a folic acid-functionalized graphene oxide (FA-GO) nanocarrier for MTX delivery. While that study laid important groundwork for FA-mediated targeting, it was limited to single-drug delivery and did not explore combination chemotherapy or the biophysical responses of cancer cells. In contrast, the present study introduces a dual-drug delivery system in which both MTX and CP are co-loaded onto FA-functionalized GO, aiming to achieve synergistic cytotoxicity and improved targeting via folate receptor-mediated uptake. Additionally, this work extends the characterization of the delivery system by including Franz diffusion modeling, cell stiffness analysis, and comparative evaluation of single- versus dual-drug formulations. To the best of the authors' knowledge, this is the first study to investigate the combined loading of MTX and CP onto a FA-functionalized GO carrier. Accordingly, the synergistic cytotoxic effects of the dual-drug system were assessed on MDA-MB-231 breast cancer cells and compared with the effects of single-drug-loaded systems.

2. Materials and Methods

2.1. Materials

The synthesis chemicals used in this study, including graphene flake (mesh size 300), ethanol, methotrexate, cyclophosphamide, sulfuric acid (H_2SO_4), potassium permanganate ($KMnO_4$, 99.9%), phosphoric acid (H_3PO_4), and hydrogen peroxide (H_2O_2, 30%), were acquired from Merck and Sigma-Aldrich (St. Louis, MO, USA). The source of folic acid was Ruber Biotechnology, located in Ankara, Turkey. The American Type Culture Collection provided the MDA-MB-231 cell line (ATCC). Gibco (New York, NY, USA) provided the fetal bovine serum (FBS), phosphate-buffered saline (PBS), Dulbecco's modified Eagle medium/nutrient mixture F-12 (DMEM/F-12), penicillin-streptomycin, trypsin-EDTA, and trypan blue. Santa Cruz Biotechnology (Dallas, TX, USA) provided XTT (2,3-bis-(2-methoxy-4-nitro-5-sulfophenyl)-2*H*-tetrazolium-5-carboxanilide) and phenazine methosulfate (PMS).

2.2. Synthesis of Graphene Oxide

The synthesis materials used in this work, including graphite flake (mesh size 300), hydrogen peroxide (H_2O_2 30%), potassium permanganate ($KMnO_4$, 99.9%), sulfuric acid (H_2SO_4), and phosphoric acid (H_3PO_4), were acquired from Merck and Sigma-Aldrich. To put it briefly, 1 g of $NaNO_3$ and 2 g of graphite were placed in a flask at 0 °C. After that, the mixture was agitated for 30 min at 5 °C with 50 mL of concentrated H_2SO_4. The reaction system was then gradually filled with 7 g of $KMnO_4$ over the course of 1 h, all the while maintaining the mixture's temperature below 20 °C. After that, the mixture was agitated for 2 h at 35 °C. Once 90 mL of deionized distilled (DD) water was gradually added to the solution, the reaction system's temper-

ature immediately increased to 70 °C. Eventually, a vivid yellow suspension formed in the reaction system after 7 mL of 30% H_2O_2 and 55 mL of DD water were added. Filtration was used to isolate the GO, which was subsequently distributed in DD water after being cleaned three times with diluted HCl (3%). In order to exfoliate GO, 200 w of sonication was applied to DD water at room temperature for 1 h, producing homogenous GO dispersions.[38]

2.3. Production of Cyclophosphamide (CP), Methotrexate (MTX)-Loaded Folic Acid (FA)-Linked Graphene Oxide (GO) Drug Delivery System

The anticancer medication was loaded by combining 1 mL of MTX (100 µg/mL; Sigma-Aldrich) with 4.0 mL of GO in buffer solution (25 µg/mL) and letting it sit at room temperature in the dark for 48 h. Folic acid (FA) was conjugated to the surface of graphene oxide (GO) via a passive adsorption method. In accordance with previously published methods,[39] 0.08 g of FA was added to the GO dispersion and mixed with 12 mL of distilled water. The mixture was stirred under dark conditions for 24 h at room temperature to promote binding between the functional groups on GO and FA.

The anticancer drug was loaded by mixing 4.0 mL of GO in buffer solution (25 µg/mL) with 1 mL of CP (100 µg/mL; Sigma-Aldrich) and allowing it to stand at room temperature in the dark for 48 h. According to the literature, GO and FA molecules were conjugated.[39] The ready GO and 0.08 g of FA were mixed together. Twelve milliliters of water were added to the mixture. Stirring the mixture for a full day in the dark was necessary for binding.

The anticancer medicine was loaded by mixing 4.0 mL of GO in buffer solution (25 µg/mL) with 0.5 mL of MTX (100 µg/mL; Sigma-Aldrich) and 0.5 mL of CP (100 µg/mL; Sigma-Aldrich) for 48 h at room temperature in the dark. According to the literature, FA molecules were conjugated to the GO.[39] The ready GO was mixed with 0.08 g of FA. Twelve milliliters of water were added to the blend. The mixture was left to stir in the dark for 24 h for binding. The GO, MTX, CP, MTX-FA-GO, CP-FA-GO, and CP-MTX-FA-GO nanostructures are the working groups discussed in this study (Figure 1). For the CP/MTX/FA/GO drug delivery system, an in vitro release kinetics investigation was conducted. Here, the CP/MTX combination's release kinetics efficiency was measured and contrasted. In addition, kinetic models were acquired for the CP/MTX/FA/GO system, and their efficacy was evaluated.

2.4. Characterization of GO and Drug Delivery Systems

2.4.1. Particle Size and Zeta Potential Analysis

Using dynamic light scattering on a Zetasizer Nano ZS (Malvern Instruments Ltd., Malvern, Worcestershire, UK), the zeta potential of the GO and CP/MTX/FA/GO was determined. Measurements were performed three times per sample on newly prepared GO and CP/MTX/FA/GO after all samples had been diluted 100 times (v/v).

2.4.2. Morphology of the GO and Drug Delivery Systems

GO, MTX/FA/GO, CP/FA/GO, and CP/MTX/FA/GO were imaged with Thermo Scientific Apreo 2S. 10 µL of supernatants were dropped on TEM grids after centrifugation (5000 rpm; 1 min) of suspensions. Ted Pella carbon Type B TEM grids were used in analysis. Bright field and dark-field transmission images were obtained by using a STEM detector equipped in FE-SEM.

2.4.3. Fourier Transform Infrared Spectroscopy (FTIR)

Bruker Tensor 27 (Karlsruhe, Germany) FTIR spectrophotometer (ATR-FTIR) was utilized to obtain Fourier transform infrared spectra of all materials. All the spectra were recorded in absorption mode at 4 cm^{-1} resolution, covering a wavelength range of 4000–500 cm^{-1}.

2.4.4. Differential Scanning Calorimetric Analysis (DSC)

The samples' thermal properties were assessed by DSC (SDT Q600, TA Instruments, New Castle, DE, USA) under nitrogen gas flow. Samples weighing 5–8 mg were carefully weighed, placed inside metal vials, and sealed. The sealed samples were heated at a rate of 10 °C/min between 20 and 250 °C, with a nitrogen flow rate of 20 mL/min.

2.5. In Vitro Study: Franz Diffusion Drug Delivery Kinetics

The most popular in vitro method for determining dermal absorption involves coating a skin sample's surface with an adequate formulation of the active substance.[40,41] The Franz diffusion device was employed for the majority of CP/MTX/FA/GO dissolution test techniques.[42,43] The sample active substances for CP/MTX/FA/GO were applied to the membranes using Franz diffusion cells. The Franz device's membrane is situated in its center. The samples of the CP/MTX/FA/GO drug delivery system were put on the membrane. The sample (1.5 mL) to be studied was inserted through the upper part of the cells, and media (2.5 mL) was supplied to the lower section of the cells. The experiment was conducted with constant speed mixing and a constant ambient temperature of 37 °C. 2.5 mL of the sample was removed from the lower section at the 15 and 30 min marks, as well as the 1st, 2nd, 4th, 6th, 8th, 24th, 30th, 36th, 42nd, and 48th hours. The sample was then replaced with fresh medium that had been heated to 37 °C. The trial was carried out once more. HPLC was used to measure the amount of active ingredient in the samples that were collected. Plotting the percentage cumulative amount of active substance passing through the cells versus time allowed for the calculation of the percentage cumulative amount passed after a full day. CP/MTX/FA/GO cumulative mass losses were statistically examined using the Minitab 19 software. The following equation were used to compute the encapsulation efficiency and drug loading of MTX and

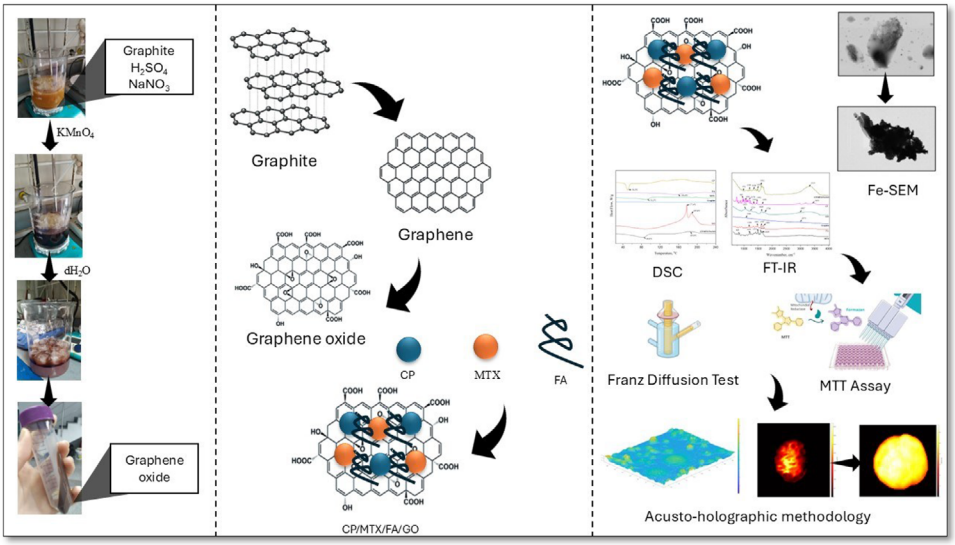

Figure 1. Experimental setup illustrating the synthesis of graphene oxide (GO), loading of cyclophosphamide (CP) and methotrexate (MTX), functionalization with folic acid (FA), and characterization of the resulting nanocarrier. The schematic also outlines the methods used to evaluate the effects of the CP/MTX/FA/GO system on MDA-MB-231 breast cancer cells. CP: cyclophosphamide, MTX: methotrexate, FA: folic acid. GO: graphene oxide.

CP.

$$EE\% = \frac{(\text{Total concentration of MTX} - \text{Total concentration of free MTX})}{\text{Total concentration of MTX}} \times 100 \quad (1)$$

The drug release kinetics of CP/MTX/FA/GO was examined using MATLAB R2023a. The zero-order model (Equation (2)), first-order model (Equations (3)–(4)), Korsmeyer–Peppas model (Equation 5), and Higuchi model (Equation 6) were applied to the releasing data since they are widely used in investigations on drug release kinetics.[44,45]

$$Q = Q_0 + Kt \quad (2)$$

$$\frac{d\,(100 - Q)}{dt} = -K\,(100 - Q) \quad (3)$$

$$Q = 100 - (100 - Q_0)\ e^{-Kt} \quad (4)$$

$$Q = K log\ (t) + Q_0 \quad (5)$$

$$Q = Q_0 + K\ t^{0.5} \quad (6)$$

Here, cumulative drug release (%) represents the total amount of drug released over time; the initial drug release refers to the amount released at the beginning of the experiment; the rate constant corresponds to the specific model applied; and time indicates the duration of the release study.

The model's performances were evaluated by calculating the R^2 and root-mean-square error (RMSE) values (Equations (7) and (8)).[46,47] The R^2 value quantifies the level of correlation between the model and the data, while the RMSE calculates the average deviation between the model's predictions and the actual values, which assesses the accuracy of the model in estimating the target value.[48]

$$R^2 = 1 - \left[\frac{\sum_{i=1}^{m}(y_i - \hat{y}_i)^2}{\sum_{i=1}^{m}(y_i - \bar{y})^2}\right] \quad (7)$$

$$RMSE = \sqrt{\frac{\sum_{i=1}^{m}(y_i - \hat{y}_i)^2}{m}} \quad (8)$$

Here, represents the i^{th} experimental data point; is the corresponding value predicted by the model for the i^{th} data point; denotes the sum of all experimental data points; and is the total number of samples.

Ultimately, the acquired models were compared and evaluated based on their performance. The model that performed the best was then presented, along with its 95% prediction boundaries, to emphasize the uncertainties seen during the experiment.

2.6. Stiffness

The impact of synthesized cyclophosphamide-loaded graphene oxide, methotrexate-loaded graphene oxide, and cyclophosphamide-methotrexate-loaded graphene oxide formulations on the biomechanical properties of the MDA-MB-231 breast cancer cell line was analyzed using an acousto-holographic method.[49] Initially, the cells were seeded onto microfluidic chips integrated with transducers. Subsequently, in the setup designed for this method, signals generated by a wave generator (Siglent SDG6032X) were amplified with a voltage amplifier (Falco Systems, WMA-300) for the production of waves. These signals were then transmitted to a PZT (lead zirconate

titanate) transducer (Steminc SMBA25W73T05PV) to be converted into acoustic waves. The cells were subjected to acoustic pressure at a frequency of 10 Hz and a voltage of 75 V, inducing vibrations in the cell membrane. These vibrations were observed using a high-speed camera (CCD camera). The displacement in the cell membrane was calculated to assess cell stiffness by measuring the elasticity of control cells, cyclophosphamide-loaded graphene oxide, methotrexate-loaded graphene oxide, and cyclophosphamide-methotrexate-loaded graphene oxide groups.

2.7. Cell Culture

The MDA-MB-231 cell line was cultivated in DMEM/F-12 media supplemented with 10% FBS and 1% penicillin-streptomycin in a CO_2 incubator at 37 °C. Upon achieving confluence, the cells had been washed with PBS (pH: 7.2) and subsequently removed from the substrate utilizing trypsin-EDTA. The cells were centrifuged at 1000 rpm for 5 min, the supernatant was discarded, and the pellet was stained with trypan blue and enumerated using a Thoma chamber.

2.8. Cytotoxicity Experiment

The cytotoxic effects of pure CP, pure MTX, GO, CP-loaded FA-linked GO, MTX-loaded FA-linked GO, and MTX- and CP-loaded FA-linked GO on MDA-MB-231 breast cancer cells were investigated by the XTT (2,3-Bis-(2-Methoxy-4-Nitro-5-Sulfophenyl)-2H-Tetrazolium-5-Carboxanilide) method. The 70–80% confluent cells were seeded into 96-well cell plates and incubated for 24 h, and the cells were allowed to become confluent by adhering to the plate surface. After incubation, experimental groups in the concentration range of 0–80 µg/mL were added to the cells, and the cells were incubated for 24 h at 37 °C in an incubator containing 5% CO_2. Medium without active substance was used as the control group, and the experiment was carried out with at least four repetitions. After incubation, a 0.4 mg/mL XTT solution was prepared using DMEM F12, XTT powder, and *N*-methyl dibenzopyrazine methyl sulfate (PMS). 100 µL of the prepared solution was added to the microplates in each well, and the microplates were incubated for 4 h. After incubation, the absorbance value of each well was measured at a wavelength of 450 nm using a multi-microplate reader. The absorbance values obtained were converted into percent cell viability for each concentration using the following Equation (9).

$$\text{Cell Viability (\%)} = \left(\frac{\text{Absorbance}}{\text{Absorbance Control}}\right) \times 100 \quad (9)$$

2.9. Statistical Analysis

All experiments were conducted in triplicate, and data are presented as mean values accompanied by standard deviation. Statistical evaluations were carried out using SPSS Statistics Software (IBM, version 20, Armonk, NY, USA). To assess differences between group means, one-way ANOVA was applied, followed by Tukey's post hoc test for multiple comparisons. A *p*-value of less than 0.05 was considered indicative of statistical significance.

3. Results and Discussion

3.1. Zeta Potential and Morphology of the GO and Drug Delivery Systems

The electric charge on the surface of particles in a colloidal system is measured by the zeta potential. It can provide insight into the interactions between particles in a solution and reflects the stability of colloids. Nanoparticles exhibiting a zeta potential between −10 and +10 mV are regarded as generally neutral, whereas those having zeta potentials exceeding +30 mV or falling below −30 mV are classified as strongly cationic and strongly anionic, respectively.[50] An elevated zeta potential value, regardless of being positive or negative, signifies enhanced stability and a greater probability of the particles resisting aggregation. A diminished zeta potential leads to increased attraction over repulsion and an uneven distribution.[51] Figure 2 shows the results of measuring the zeta potential in deionized pure water (pH = 7.0). It was found that chemically processed graphite (GO) had a negative zeta potential when it came to colloidal stability in an aqueous media (−26 mV). The existence of —COOH groups on the GO surface is most likely the cause of this negative zeta potential.[52] A slight reduction in the zeta potential of GO (−26 mV) was seen in MTX/FA/GO (−29 mV); this could potentially signify the potential creation of amide bonds between MTX and FA and GO ($p < 0.05$). A distinct increase in the zeta potential of GO (−26 mV) was seen in CP/FA/GO (−17 mV); a high zeta potential suggests that there is sufficient repulsion between the particles to stop them from aggregating ($p < 0.05$).[53] The zeta potential value of the CP/MTX/FA/GO drug delivery system produced as a combined formulation was measured as −25 mV. The measured value indicates that the produced CP/MTX/FA/GO drug delivery system is within the range of stable stability[50] and an average of MTX/FA/GO and CP/FA/GO drug delivery systems.

Field emission scanning electron microscopy (FE-SEM) was performed to examine the microstructure[54] of the GO, MTX/FA/GO, CP/FA/GO, and CP/MTX/FA/GO drug delivery systems. The FE-SEM image of GO in Figure 3a (black arrows) shows the flake-like nanosheet structure of the 2D structure of GO layers.[55] A general examination of Figure 3a,b reveals an increase in particle size, suggesting that the therapeutic agents (CP and MTX) and the targeting ligand (FA) were successfully conjugated to the GO surface. This structural expansion may be attributed to π–π stacking interactions between the nitrogen-containing groups of CP and MTX and the π-conjugated, sp^2-hybridized domains of GO. These findings confirm that the exfoliation of graphite resulted in the formation of 2D GO nanosheets. Similar morphological features have been reported in previously published studies.[55–59]

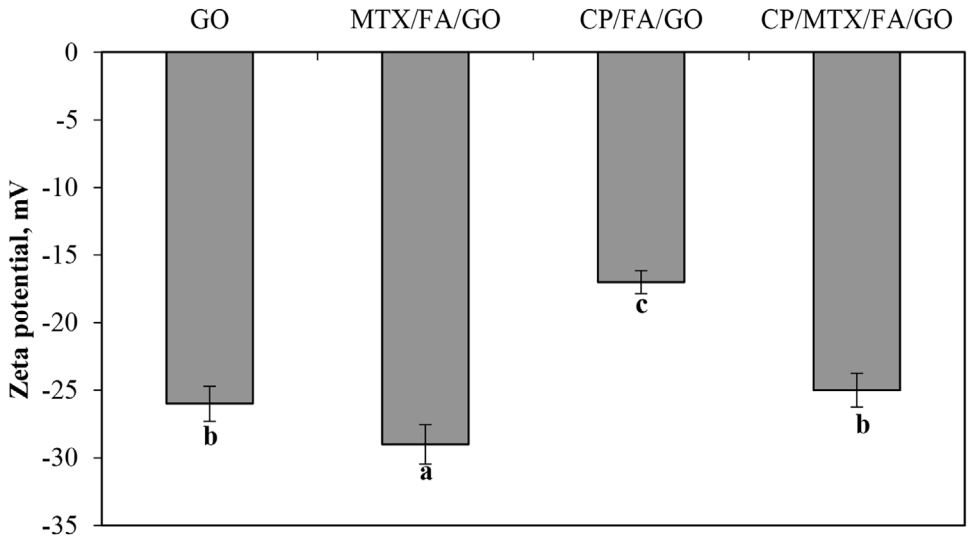

Figure 2. Zeta potential analysis of GO, MTX/FA/GO, CP/FA/GO, and CP/MTX/FA/GO drug delivery systems. CP: cyclophosphamide, MTX: methotrexate, FA: folic acid. GO: graphene oxide. Values were presented as mean ± SD ($n = 3$); means with different letters were significantly different ($p < 0.05$).

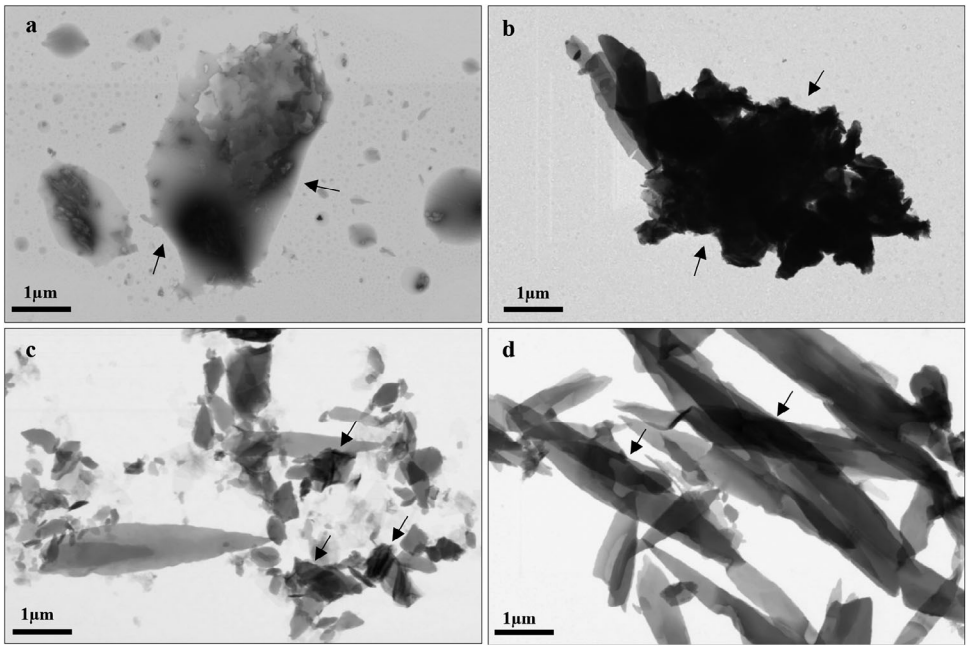

Figure 3. FE-SEM images of a) GO, b) MTX/FA/GO, c) CP/FA/GO, and d) CP/MTX/FA/GO drug delivery system. CP: cyclophosphamide, MTX: methotrexate, FA: folic acid. GO: graphene oxide.

The MTX/FA/GO FE-SEM images in Figure 3b illustrate the structures that have developed an elevated structure on these flake layers to build a 3D shape (black arrows). Additionally, the structures that have created a raised structure on these flake layers to produce a 3D shape are apparent in the FE-SEM images of CP/FA/GO in Figure 3c. Analysis of the FE-SEM image in Figure 3d reveals that the CP/MTX/FA/GO formulation exhibits a denser 3D structure compared to the GO, MTX/FA/GO, and CP/FA/GO drug delivery systems. Although the lateral dimensions of the GO-based carrier appear to be in the micrometer range based on FE-SEM images, the thickness of single-layer GO sheets is approximately 0.34–1 nm, which places the material in the nanoscale domain.[15] Due to their 2D morphology, high aspect ratio, and atomic-scale thickness, GO sheets exhibit unique physicochemical properties that allow them to circulate through the vasculature and interact with biological systems in ways distinct from conventional spherical nanoparticles.[60,61] Moreover, it is important to consider that GO's biological behavior is influenced not only by its size but also by factors such as cell type and surface charge interactions.[62] As emphasized by Salatin et al.,[63] nanoparticle size plays a critical role in determining cellular uptake, renal clearance, and biological toxicity. GO sheets can range from 10 nm to over 20 µm in lateral dimension. Smaller GO nanosheets are typically internalized via

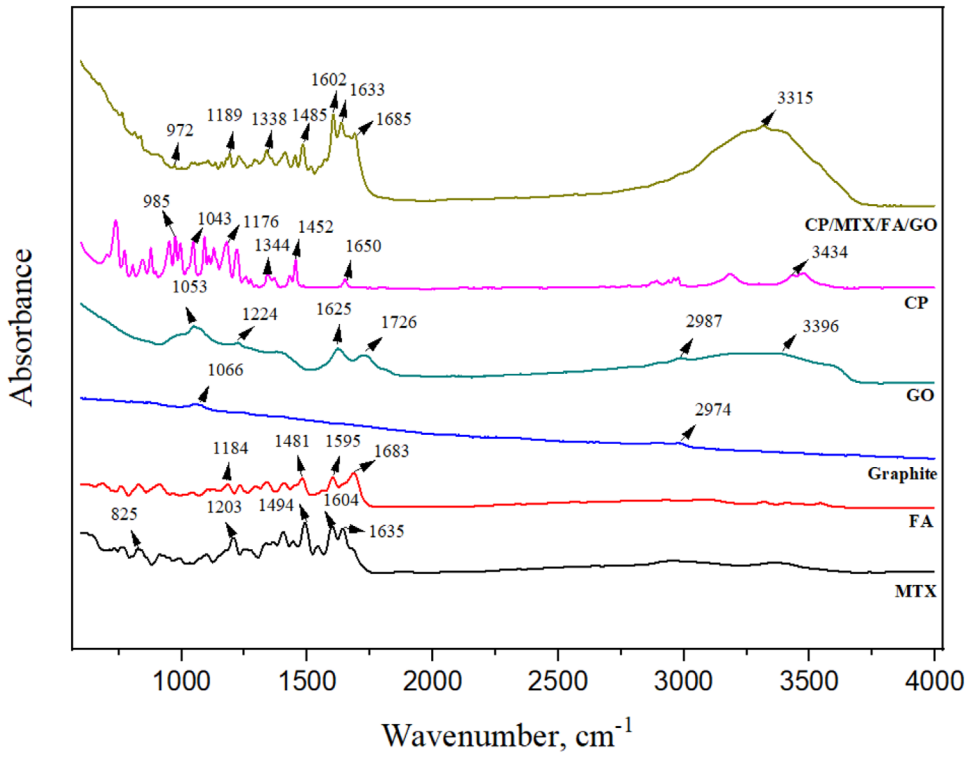

Figure 4. FTIR of pure CP, FA, MTX, GO, graphite, and CP/MTX/FA/GO drug delivery system. CP: cyclophosphamide, MTX: methotrexate, FA: folic acid. GO: graphene oxide.

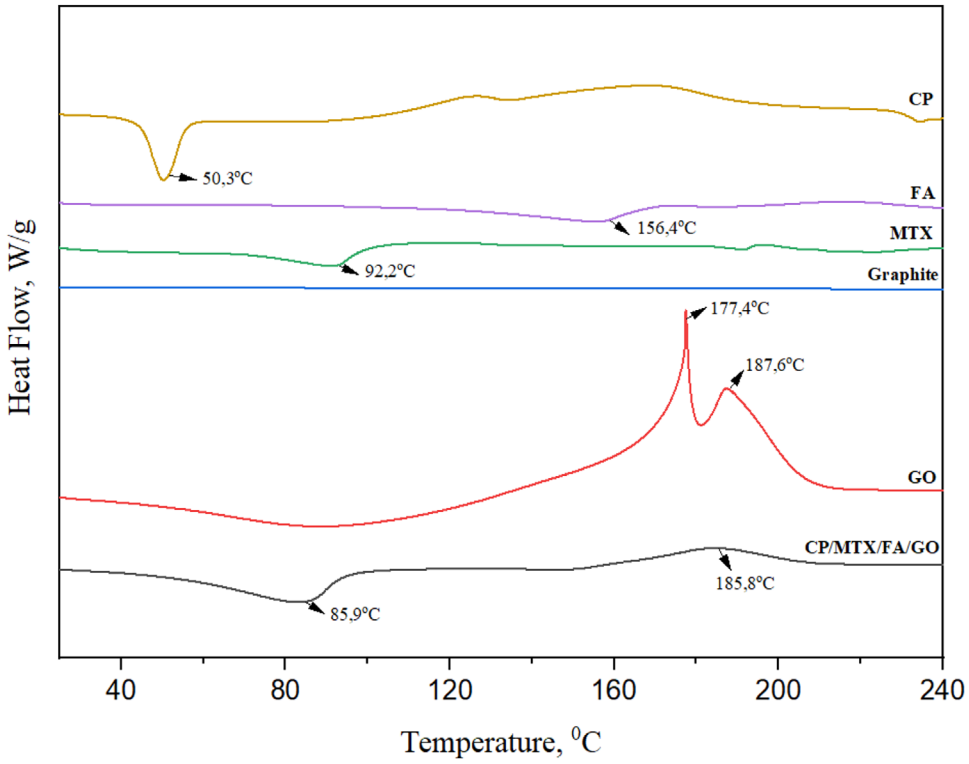

Figure 5. DTG thermograms of pure CP, FA, MTX, GO, graphite, and CP/MTX/FA/GO drug delivery system. CP: cyclophosphamide, MTX: methotrexate, FA: folic acid, GO: graphene oxide.

endocytosis, whereas larger sheets may adhere to cell membranes and be taken up through alternative mechanisms such as membrane wrapping or passive penetration.[64] Yue et al.[65] investigated the cellular uptake of 350 nm and 2 μm GO sheets in both phagocytic (e.g., macrophages) and non-phagocytic (e.g., endothelial and cancer) cells. Their results showed that uptake by non-phagocytic cells was minimal due to electrostatic repulsion between the negatively charged GO and the cell surface. In contrast, phagocytic cells showed efficient uptake of GO, independent of lateral size, as also confirmed by Mendes et al.[66] Importantly, Pourjavadi et al.[19] demonstrated a dual-drug-loaded GO system composed of micrometer-sized sheets, which was still classified as a nanocarrier due to its nanoscale thickness and effective functional behavior in drug delivery. Therefore, although our GO-based carrier has a relatively large lateral dimension, we suggest that it can still be reasonably defined as a nanocarrier based on its 2D structure, atomic thickness, surface chemistry, and partial cellular interaction mechanisms. Nevertheless, it is worth noting that the relatively large lateral dimensions of the GO sheets in our CP/MTX/FA/GO system may pose a limitation for uptake efficiency in non-phagocytic cancer cells, which should be considered in future in vivo evaluations.

3.2. Physicochemical Analysis

3.2.1. FTIR Analysis

The technique known as Fourier transform infrared spectroscopy (FTIR) is used to investigate the existence of different functional groups in chemical constituents and manufactured materials. After oxidation, more oxygen-containing functional groups should be present in GO, the oxide form of graphite.

For graphite, only a few peaks can be seen in Figure 4 at 2974 and 1066 cm^{-1}. When observing GO, the strong, broad peak that appears at 3396 cm^{-1} indicates that an O—H bond (hydroxyl group) is present. Furthermore, at wavelengths of 1224 and 1053 cm^{-1}, the C—O—C stretching (epoxy group) and the —C═O stretching (—COOH group) may be observed.

All of these groups—carboxylic, hydroxyl, epoxide, and carbonyl—may suggest that oxygen atoms (O) are attached to GO, indicating the effective synthesis of GO.[18] The presence of C═C, C═O, and O—H bonds in GO is confirmed by the peaks at 1625, 1726, and 3396 cm^{-1}, as depicted in Figure 4. The FTIR spectrum of CP demonstrates characteristic bands at 3434 and 985 cm^{-1} for NH and 1176 cm^{-1} for C—N stretching, with the wavenumber 1043 cm^{-1} indicating the O═P—OH group. P═O was associated with the peak at 1650 cm^{-1}. At 1344 cm^{-1}, the appearance of the —CH_2Cl bond was detected.[67] The characteristic absorption band associated with C═O stretching at 1635 cm^{-1} is visible in the FTIR spectra of MTX. In the spectral range of 1494–1604 cm^{-1}, bands attributable to N—H bending from the amidic group are visible. Additional noticeable bands, including 1203 cm^{-1}, are associated with —C—O extending from the carboxylic group, whereas 825 cm^{-1} corresponds to C—H bonds on an aromatic ring.[68,69] GO is a 2D nanostructure made of hybridized carbon with hydroxyl, carboxyl, and epoxide functional groups on the surface of sp^2. The sp^2-hybridized π-conjugated structure of graphene oxide sheet can form $\pi-\pi$ stacking interactions with nitrogen groups of CP and MTX.[67] The amine (NH_3) and oxygen groups of CP and MTX may also generate a strong hydrogen bond contact with hydroxyl (OH) and carboxyl (COOH) groups in GO.[70] There are characteristic peaks in GO corresponding to C═C and C═O stretching at 1625 and 1726 cm^{-1}, respectively. Additionally, the C═O stretching in FA appears at 1683 cm^{-1}, and N—H bending vibrations are observed at 1650 and 1635 cm^{-1} for CP and MTX, respectively. In the CP/MTX/FA/GO formulation, new or shifted bands were observed at 1602, 1633, and 1685 cm^{-1}, which may be attributed to strong hydrogen bonding or amide-like interactions between the —COOH groups of GO, the amino groups in CP and MTX, and functional groups in FA. These shifts suggest a successful physical interaction and possible partial conjugation of FA onto the GO surface. This is supported by the presence of a distinct C═O stretching band at 1683 cm^{-1} (from FA) and is consistent with previously reported non-covalent adsorption mechanisms via hydrogen bonding and electrostatic interactions.[71,72]

3.2.2. DSC Analysis

The compounds' crystallinity, amorphism, and potential physicochemical interactions were assessed by DSC (Figure 5). Graphite powder did not exhibit any peaks related to decomposition. Conversely, GO exhibited a similar pattern to a prior work,[18,73] with an exothermic peak between 177.4 and 187.6 °C. The decomposition peaks identified in GO, unlike in graphite powder, are due to chemical interactions with oxygen. The breakdown of oxygenic groups into CO_2 as a result of the catalytic dehydration of epoxy (C—O—C), hydroxyl (O—H), and carboxyl (—COOH) bonds is responsible for the GO decomposition peaks seen at 177.4 and 187.6 °C.[18,74]

An endothermic peak was visible on the DSC curves for CP, MTX, and FA, respectively, at 50.3, 92.2, and 156.4 °C. CP has also been shown to give an endothermic peak at 50.3 °C in previous studies.[75] At 85.9 and 185.8 °C, there were endothermic peaks in the combination drug delivery system. There was no observation of the melting peaks of CP and MTX at 50.3 and 92.2 °C in the drug delivery system CP/MTX/FA/GO. It is possible that CP and MTX bind to GO in a noncrystalline state on the CP/MTX/FA/GO surface because the DSC analysis did not reveal any phase transitions caused by them.[76] The absence of a melting peak corresponding to free FA in the DSC thermogram further supports the covalent or strong associative incorporation of FA into the GO matrix. The primary metabolite of CP, namely 4-hydroxy-CP, has high pharmacological activity but is a very unstable compound.[75] As seen in the DSC thermogram, CP, which has a melting peak at 50.3 °C, was made into a combined formulation (CP/MTX/FA/GO) when the melting peak of the formulation increased to 85.9 °C. This may indicate that the stability of CP was also increased.

The structural and thermal analyses confirmed the successful incorporation of CP and MTX into the GO-based nanocarrier

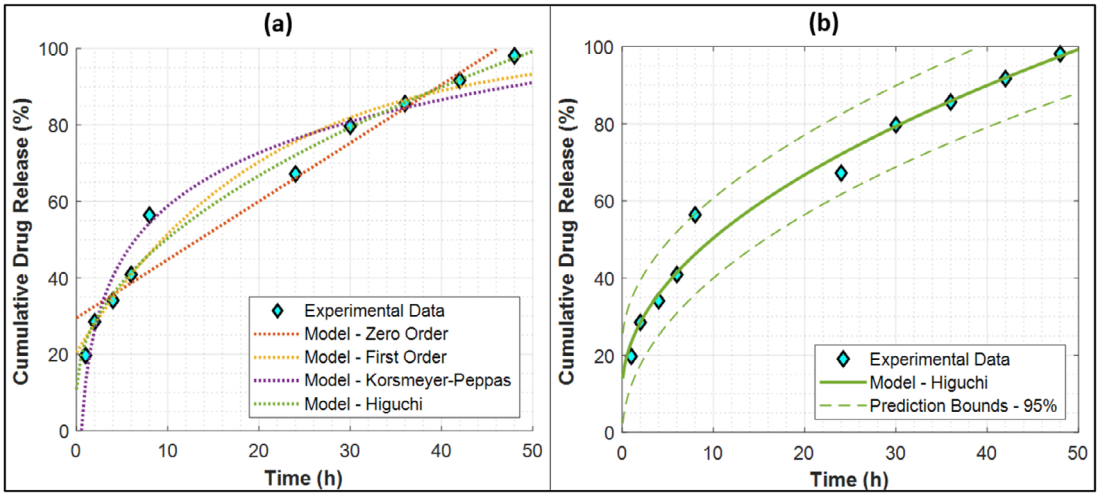

Figure 6. The drug release kinetics of CP/MTX/FA/GO drug delivery system with respect to a) all kinetic models and b) the best-performing kinetic model with its 95% prediction bounds. CP: cyclophosphamide, MTX: methotrexate, FA: folic acid, GO: graphene oxide.

system and provided indirect evidence of product purity. In the FTIR spectra of the final CP/MTX/FA/GO formulation, characteristic amide bond peaks were observed at 1602, 1633, and 1685 cm^{-1}, which were absent in the spectra of the individual components. These peaks indicate covalent bonding between the —COOH groups of GO/FA and the —NH groups of CP and MTX, suggesting that the drugs were effectively conjugated to the GO matrix and that no free drug molecules remained. Complementary thermal analysis via DSC further supported this conclusion. While free CP and MTX displayed distinct endothermic melting peaks at 50.3 and 92.2 °C, respectively, these peaks were no longer present in the CP/MTX/FA/GO thermogram. Instead, two new endothermic transitions were detected at 85.9 and 185.8 °C. The absence of the original melting points and the emergence of new thermal events indicate that CP and MTX are present in an amorphous or molecularly dispersed form, rather than in a crystalline state. This transformation suggests enhanced drug stability and confirms successful loading within the GO matrix, further supporting the structural integrity and purity of the final nanocarrier system.

3.3. In Vitro Study: Franz Diffusion Drug Delivery Kinetics

The goal of this study's comparison of mathematical models with Franz cells is to evaluate the release and permeability profiles of various drug combinations, formulations, and delivery strategies. This has aided in determining the best drug delivery techniques. Primary mechanisms for solute transport from drug-containing polymeric matrices include material degradation, polymeric matrix swelling, and the drug system's diffusion biodegradability.[77]

Using mathematical models to analyze the release kinetics of medicines from various formulations is crucial for understanding the pace and extent of drug release over a specific period of time. In order to determine the cumulative drug release (%) over time, various mathematical models, including zero-order, first-order, Korsmeyer–Peppas, and Higuchi models, were applied to the experimental data. The table provides the model parameters and performance indicators for the models. The correlation coefficient (R^2) was used to assess the efficacy of various release regimes. The best mathematical model to represent the CF/MT release kinetics was found to have the highest correlation coefficient.[77]

It is evident that the Higuchi model outperforms other models, as it has the highest R^2 value and the lowest RMSE value. The resulting models are compared to the experimental data in Figure 6a to further confirm the exceptional performance of the Higuchi model. The experimental results strongly support the Higuchi model as the most accurate representation of the drug release kinetics for CP/MTX/FA/GO nanomaterials, which also indicates that Fickian diffusion is the dominant mechanism for the drug release, where the drug release is driven by a concentration gradient through the porous structure of the matrix.[78,79] The strong linear correlation observed with the Higuchi model ($R^2 > 0.99$), along with low RMSE values, supports this mechanism. Moreover, during the experimental period, no significant swelling, degradation, or relaxation of the GO-based carrier was observed, which typically characterizes non-Fickian (anomalous) diffusion behaviors.[80,81] Therefore, based on both model fitting and empirical observation, the drug release behavior is best described as classical Fickian transport, in which diffusion is the primary rate-controlling step.[82] Figure 6b displays the Higuchi model that has the highest performance, along with its 95% prediction boundaries. Upon investigation of the release kinetics of CP/MTX/FA/GO, it was observed that the maximum release of CP reached 98.7% after 48 h. In a similar study we conducted before, it was found that MTX release was in accordance with the Higuchi model in the Franz diffusion mathematical model.[18] Findings from release experiments demonstrate that the CP/MTX/FA/GO combined drug delivery system loaded with CP/MTX effectively delivers consistent amounts of CP for 48 h (Table 1).

Table 1. Model parameters and performance indicators are used to analyze the drug release kinetics of CP/MTX/FA/GO drug delivery system.

Models	Parameters		Metrics	
	K	Q_0	R^2	RMSE
Zero order	1.5314	29.7193	0.9419	7.2659
First order	0.0499	20.5980	0.9632	5.7853
Korsmeyer–Peppas	20.1523	12.6441	0.9565	6.2863
Higuchi	12.6549	10.4265	0.9837	4.1797

3.4. Stiffness

One of the fundamental biomechanical characteristics of a cell, cell stiffness is linked to the characteristics of cancer cells' motility, invasion, and metastasis. Prior research has demonstrated that cell stiffness, as measured by AFM devices, can serve as a marker for the potential for metastasis and the advancement of cancer.[83] The cell stiffness of various cancer forms varies, and it has also been shown that there is a correlation between greater invasive capacity and reduced cell stiffness.[84]

Figures 7 and 8 compare the changes in cancer cell stiffness following treatment with the generated formulation. The outcomes demonstrate that, in comparison to the control group, the stiffness of cancer cells treated with the formulation containing both CP and MTX reduced. The average cell stiffness was measured as 0.9141 kPa for the control group, 0.3569 and 0.7548 kPa for cells treated with only MTX and CP, and 0.0913 kPa for cells treated with the CP/MTX/FA/GO combined drug delivery system. In particular, the administration of MTX and CP together significantly weakened the cell wall, while FA also increased cell permeability. Cytotoxicity results also confirmed that the combined formulation had the highest cytotoxic effect on cancer cells. Fraczkowska et al.[85] studied the stiffness effects of DOX on acute myeloid leukemia cancer cells and showed that doxorubicin reduced the mechanical strength by affecting the mechanical properties of cell structures. They said that this situation is due to the interaction of anticancer drugs with nuclear structures, especially nucleic acids, and that DOX inhibits actin polymerization, and thus cytoskeletal modification may have caused the reduction of cell mechanical strength. It can also be said that the decrease in cell mechanics is due to the incorporation of combined drugs into the cell lipid membrane under the leadership of FA. Li et al.[86] examined the effect of MTX on cell biomechanical properties and stated that MTX-treated cells underwent morphological changes such as lost filamentous structures, and as a result, their mechanical structures weakened. In addition, in another study we showed that the mechanical properties of cancer cells treated with MTX combination were weakened.[18]

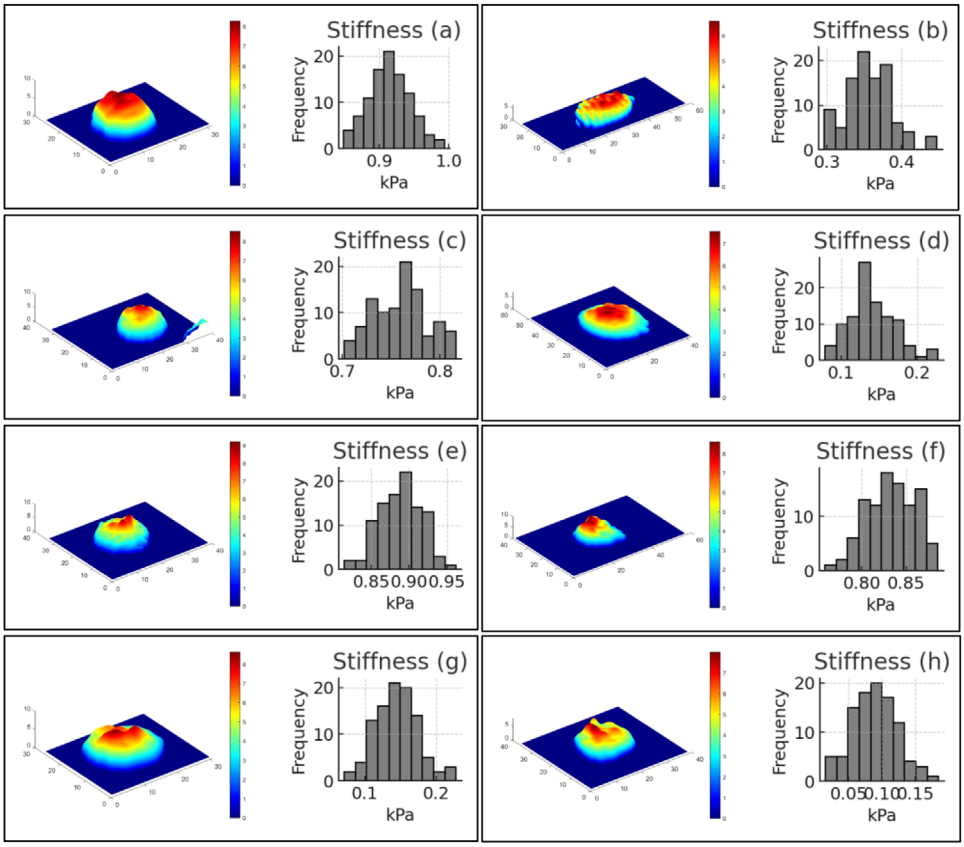

Figure 7. 3D images and stiffness histogram of the membrane structure of MDA-MB-231 breast cancer cells. a) Non-treated control group, treated with b) MTX, c) CP, d) GO materials, e) CP/FA/GO, f) MTX/FA/GO, g) CP/MTX/GO, and h) CP/MTX/FA/GO drug delivery systems. CP: cyclophosphamide, MTX: methotrexate, FA: folic acid. GO: graphene oxide.

Research Article
doi.org/10.1002/slct.202500457

Chemistry Europe
European Chemical Societies Publishing

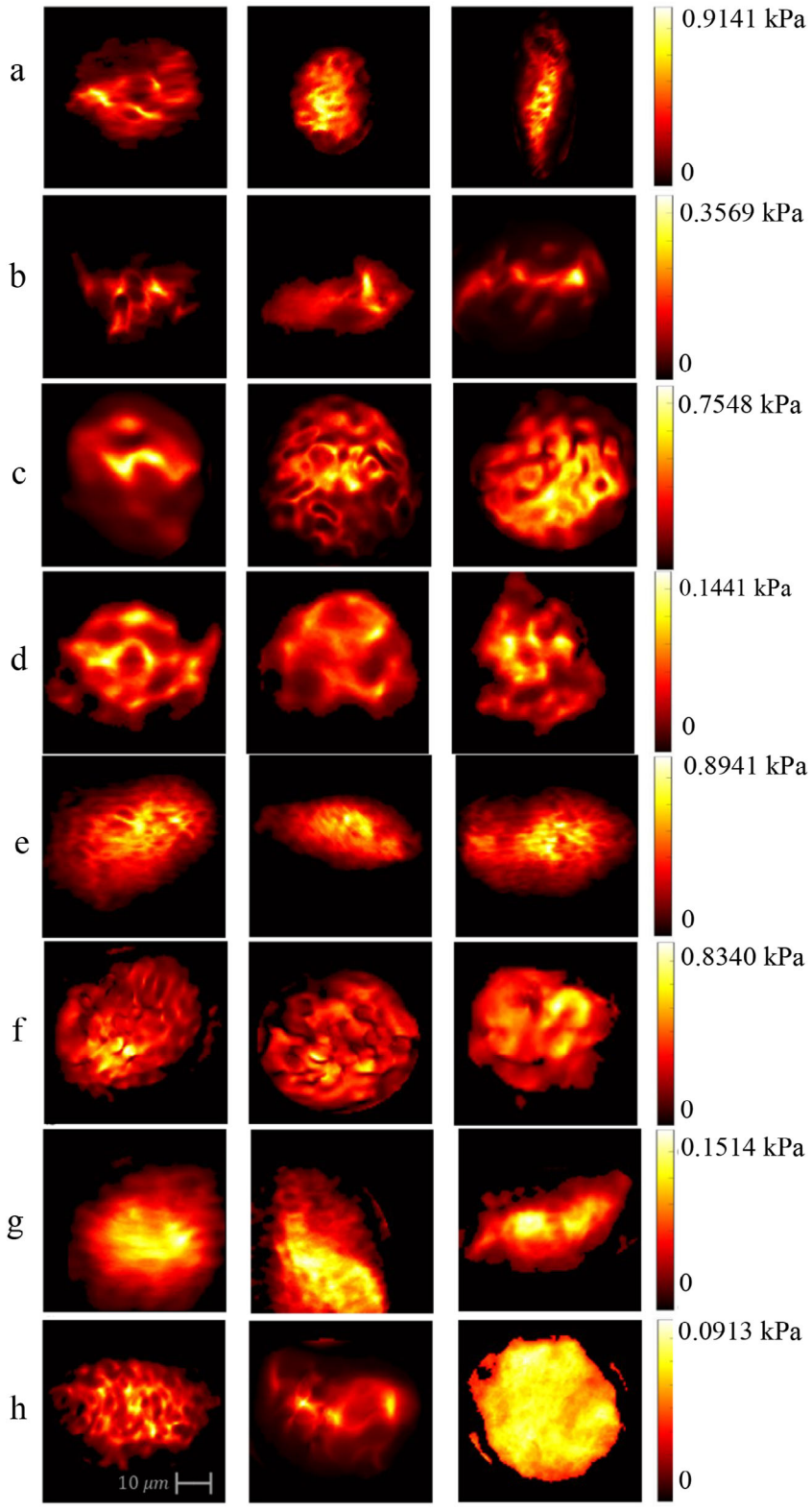

Figure 8. The effect of samples on the membrane stiffness of MDA-MB-231 breast cancer cells. a) Non-treated control group, b) MTX, c) CP, d) GO, e) CP/FA/GO, f) MTX/FA/GO, g) CP/MTX/GO, and h) CP/MTX/FA/GO. CP: cyclophosphamide, MTX: methotrexate, FA: folic acid, GO: graphene oxide.

3.5. Cell Culture and Cytotoxicity Analysis

The cytotoxicity and antiproliferative effects of pure CP, MTX, GO, and complexs of CP/FA/GO, MTX/FA/GO, and CP/MTX/FA/GO samples were investigated using an MTT assay test against MDA-MB-231 breast cancer cell line, and cell viability (%) after 24 h of incubation are given in Figure 9. When the results were examined, it was seen that pure CP drug did not reduce cell viability at concentrations of 1, 5, 10, 20 and 30 µg/mL compared to the control, and at concentrations of 40, 50, 60, 70 and 80 µg/mL, cell viability decreased by 15%, 30%, and 33%, respectively. It was found to cause a 36% and 37% reduction (Figure 9a).

Pure MTX drug did not cause a significant decrease in cell viability between concentrations of 1 and 30 µg/mL compared to the control group. At concentrations between 40 and 80 µg/mL, it showed a cytotoxic effect by killing 10%, 25%, 30%, 36%, and 38% of breast cancer cells, respectively (Figure 9b). When Figure 9c is examined, it is seen that GO material causes an average 12%–13% decrease in cell viability only at concentrations of 60, 70, and 80 µg/mL. Concentrations of the substance between 1 and 30 µg/mL increased cell viability values by 15%–20% compared to the control ($p < 0.05$). Cyclophosphamide-loaded graphene oxide (CP/GO) material showed an average of 20% more toxic effect on cells at concentrations of 20 and 30 µg/mL compared to pure CP. This shows that the formulation with GO causes the concentration range in which pure CP has anticancer activity to expand. In the concentration range of 40 to 80 µg/mL, it was observed that both substances exhibited cytotoxic effects on similar cancer cells, causing a decrease of approximately 30%–40% in cell viability (Figure 9d). When the MTX/FA/GO formulation was compared to pure MTX, although they showed similar toxicity at the first two concentrations, MTX/FA/GO showed 17% and 23% more toxic effects than pure MTX at concentrations of 30 and 40 µg/mL, respectively. MTX/FA/GO caused more toxic effects than pure MTX, causing the death of nearly 47% of cancer cells, especially at concentrations between 40 and 80 µg/mL (Figure 9e). This could be related to GO and MTX's synergistic effects. Furthermore, since cancer cells overexpress folate receptors,[87] adding FA to the MTX/FA/GO micro-material guarantees that the structure becomes target-specific. Furthermore, many sources have reported[88] that, depending on concentration, FA may be able to treat breast cancer. The folate receptor (FR) located on the cell surface is used in the receptor-facilitated endocytotic route to transport FA into cells. FR receptors are known to be overexpressed in a number of cancerous tissues, such as lung, ovary, cervix, kidney, and breast tumors.[89] Various folic acid-conjugated nanocarriers have been produced in various studies to provide better drug uptake by cancer tissue.[90,91] In our previous study,[18] it was shown that functionalization of the drug delivery system with FA is an effective option to increase the efficacy of the MTX anticancer drug and to gain a target-specific structure.

It was observed that the CP/MTX/FA/GO formulation obtained by combining CP and MTX with FA caused a 43% decrease in cell viability, causing a very high toxic and synergistic effect against breast cancer cells (Figure 9f). Compared to MTX/FA/GO, it was found that it reduced cell viability by an average of 10% more, especially at concentrations of 20 and 30 µg/mL, and had a more cytotoxic effect on cancer cells in this concentration range. It has been observed that it has an average of 10% more toxic effect than CP/FA/GO in the concentration range of 30 to 80 µg/mL ($p < 0.05$).

As a result, formulations containing GO showed more cytotoxic effects on cancer cell lines than pure drugs. In addition, it was observed that the formulation in which CP and MTX were used together (CP/MTX/FA/GO) showed a higher antiproliferative effect on breast cancer cell line compared to the MTX/FA/GO and CP/FA/GO formulations in which the drugs were used alone. The CP/MTX/FA/GO system exhibited an average of 17%–23% higher cytotoxicity than the MTX/FA/GO system at 30 and 40 µg/mL concentrations and a maximum of 47% cell viability reduction at higher concentrations, indicating a synergistic enhancement of therapeutic efficacy in the dual-drug formulation. Compared to our previous study using a single-drug MTX/FA/GO system, the co-loading of CP in the current CP/MTX/FA/GO formulation resulted in significantly enhanced cytotoxicity, supporting the potential of dual-drug delivery in improving therapeutic outcomes.[18] It is known that various cancer drugs have a synergistic effect when used together.[92] Kulkarni and Rawtani[93] found that the combination of tamoxifen and doxorubicin drugs had a synergistic effect against the MCF-7 breast cancer cell line. Zhang et al.[94] loaded doxorubicin (DOX) and camptothecin (CPT) onto FA-functionalized GO and showed that GO loaded with two anticancer drugs exhibited specific targeting and remarkably high cytotoxicity to MCF-7 cells compared to NGO loaded with DOX or CPT alone. In addition, stiffness analysis showed that the combined use of CP and MTX with FA and GO increased the cytotoxic effect by changing cell mechanics. The cell wall was weakened more in CP/MTX/FA/GO application compared to free CP and MTX application, which increased drug penetration. The literature supports the finding that, as compared to GO or CP and MTX alone, the CP/MTX/FA/GO combination demonstrated a dominant anticancer activity. This is especially true given that GO has the ability to increase it. Given that combining two or more medications is a commonly used clinical practice and frequently demonstrates significantly greater therapeutic efficacy than a single medication, it is expected that controlled loading and targeted delivery of mixed anticancer drugs using these graphene-based nanocarriers will find widespread use. A comprehensive comparison of previous studies on graphene oxide-based and other nanocarrier systems is summarized in Table 2, highlighting the unique features and the advantages of our dual-drug CP/MTX/FA/GO system.

It's well established that the way cells take up particles depends a lot on their size. Generally, nanoparticles smaller than 200 nm tend to enter cells through clathrin-mediated endocytosis—a common and efficient pathway. On the other hand, larger particles, especially those above 200 nm, usually need alternative routes like macropinocytosis or phagocytosis to be internalized.[95,96] But these mechanisms do not work as effectively in non-phagocytic cells, such as most breast cancer cells. From a molecular pharmacology point of view, this means that the cytotoxic effects observed in our study may not be entirely

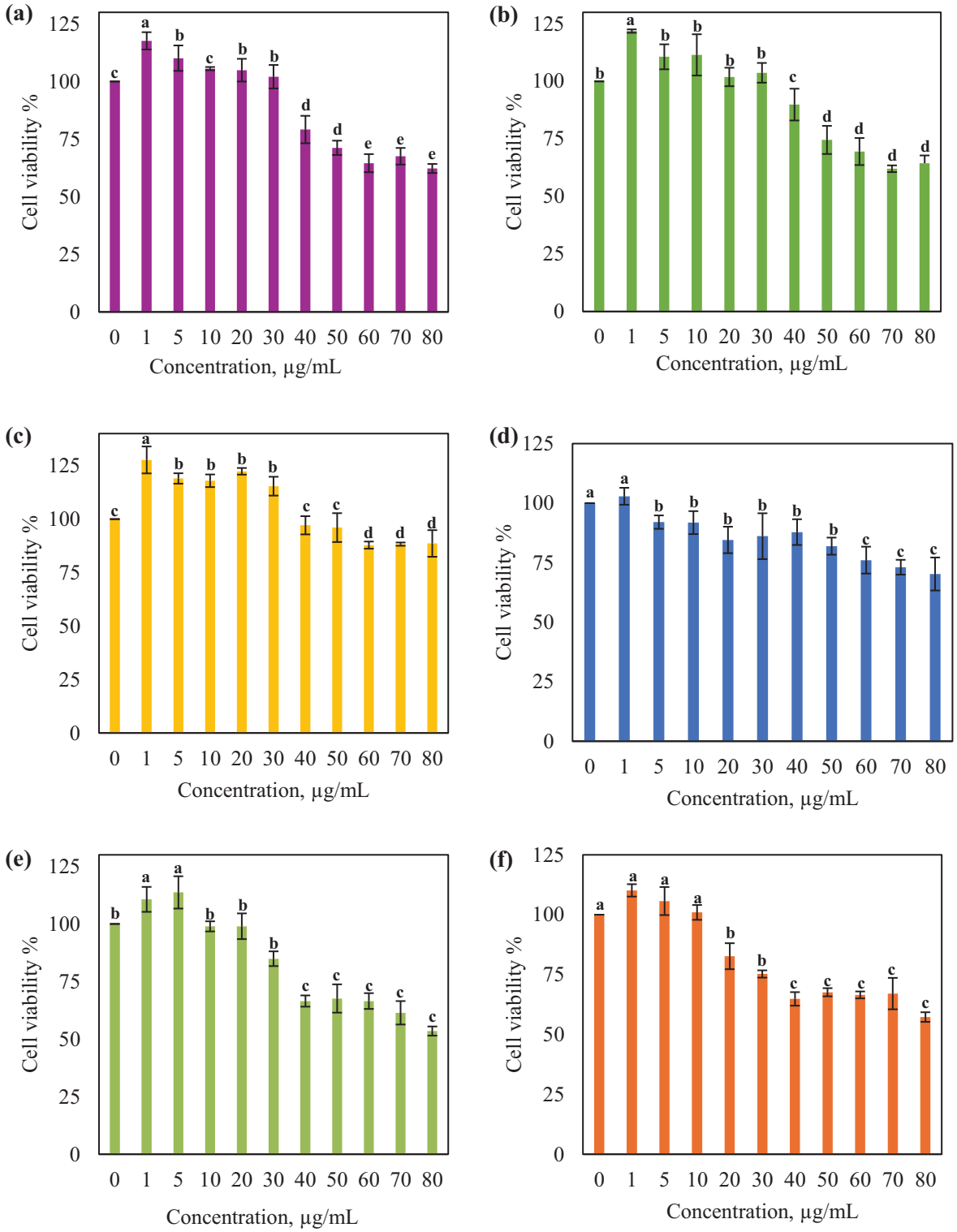

Figure 9. Effect of pure a) CP, b) MTX, c) GO, and drug delivery system of d) CP/FA/GO, e) MTX/FA/GO, f) CP/MTX/FA/GO on the viability of MDA-MB-231 breast cancer cells. CP: cyclophosphamide, MTX: methotrexate, FA: folic acid, GO: graphene oxide. Values were presented as mean ± SD ($n = 3$); means with different letters were significantly different ($p < 0.05$).

due to direct intracellular delivery of the drugs. Instead, it's possible that interactions with the cell surface, changes in membrane properties, or local drug effects played a more significant role.[97]

4. Conclusion

In this study, a folic acid (FA)-functionalized graphene oxide (GO)-based dual drug delivery system co-loaded with methotrex-

Table 2. Comparison between previous studies on drug delivery systems using graphene oxide and other carriers and those used in this study.

Drugs	Carrier	Functionalization	Cancer cell line	Limitation vs our work	Reference
Tamoxifen, DOX	Niosomes	None	MCF-7	No FA targeting, no GO	[93]
DOX, CPT	GO	FA	MCF-7	No dual-drug sustained release, no stiffness analysis	[94]
MTX	GO	FA	MDA-MB-231	Single-drug only, no CP synergy	[18]
Hydrophobic and hydrophilic drugs	GO	pH-sensitive polymer	–	No FA targeting, no dual-drug synergy	[19]
Anticancer drugs	Nanoparticles	FA & Biotin	–	Not GO-based, no dual-drug synergy	[35]
Letrozole, CP	Nanoniosomes	FA	Breast cancer	Not GO-based, no mechanical analysis	[31]
DOX, MTX	GO	Polyelectrolyte layers	–	No FA targeting, no dual-drug synergy	[51]
MTX	GO	None	–	No FA, no dual-drug synergy	[37]
Anticancer drugs	MCM-41	Mesoporous silica	–	Different carrier, no GO	[32]
MTX, CP	GO	FA	MDA-MB-231	–	Present study

ate (MTX) and cyclophosphamide (CP) was successfully developed and characterized. GO was synthesized from graphite using a modified Hummers method, and its physicochemical integrity and functionalization were confirmed through FTIR and DSC analyses. The successful conjugation of CP, MTX, and FA to GO was also supported by zeta potential, DLS, and FE-SEM analyses, which revealed a stable and compact three-dimensional structure for the CP/MTX/FA/GO system.

Drug release studies demonstrated a sustained release profile with approximately 98% of MTX and CP released over 48 h. Moreover, Franz diffusion studies indicated that CP followed Higuchi model kinetics, suggesting Fickian diffusion behavior. Cytotoxicity and stiffness assays revealed that the combined CP/MTX/FA/GO formulation significantly reduced the viability and mechanical resistance of MDA-MB-231 breast cancer cells when compared to single-drug-loaded systems or free drugs. The observed decrease in cell stiffness strongly supports enhanced cellular uptake and therapeutic impact.

These findings highlight the potential of FA-targeted, GO-based dual-drug carriers in cancer treatment, offering synergistic cytotoxic effects and improved drug delivery performance. Future in vivo studies are warranted to further explore the clinical relevance and targeted therapeutic efficacy of this nanocarrier platform. In the future, the therapeutic efficiency of the system could be further improved by designing an optimized version with reduced particle size while maintaining drug-loading capacity and target specificity.

Acknowledgments

The authors acknowledge financial support from the Yıldız Technical University Scientific Research Project (No: FDK-2021-4474) provided for this work.

Conflict of Interests

The authors declare no conflict of interest.

Data Availability Statement

The data that support the findings of this study are available on request from the corresponding author. The data are not publicly available due to privacy or ethical restrictions.

Keywords: Cancer therapy · Carbon materials · Cyclophosphamide · Drug delivery · Methotrexate

[1] S. H. Hassanpour, M. Dehghani, *J. Cancer Res. Pract.* **2017**, *4*, 127–129.
[2] R. L. Siegel, K. D. Miller, A. Jemal, *CA Cancer J. Clin.* **2016**, *66*, 7–30.
[3] R. Kaur, A. Bhardwaj, S. Gupta, *Mol. Biol. Rep.* **2023**, *50*, 9663–9676.
[4] R. Siegel, D. Naishadham, A. Jemal, *CA Cancer J. Clin. ACS* **2013**, *63*, 11–30.
[5] G. Ma, G. Ning, Q. Wei, *Carbon* **2022**, *195*, 328–340.
[6] S. Rawat, R. K. Mishra, T. Bhaskar, *Chemosphere* **2022**, *286*, 131961.
[7] Q. Chen, X. Tan, Y. Liu, S. Liu, M. Li, Y. Gu, P. Zhang, S. Ye, Z. Yang, Y. Yang, *J. Mater. Chem. A* **2020**. *8*, 5773–5811.
[8] K. P. Gopinath, D. V. N. Vo, G. D. Prakash, A. A. Joseph, S. Viswanathan, J. Arun, *Environ. Chem. Lett.* **2021**, *19*, 557–582.
[9] Z. Peng, T. Zhao, Y. Zhou, S. Li, J. Li, R. M. Leblanc, *Adv. Healthcare Mater.* **2020**, *9*, 1901495.
[10] S. Zheng, Y. Tian, J. Ouyang, Y. Shen, X. Wang, J. Luan, *Front. Chem.* **2022**, *10*, 990362.
[11] V. Vitus, F. Ibrahim, W. S. W. K. Zaman, *Polymers* **2021**. *13*, 4058.
[12] J. Khan, S. A. Momin, M. Mariatti, *Carbon* **2020**. *168*, 65–112.
[13] T. Mathew, R. A. Sree, S. Aishwarya, K. Kounaina, A. G. Patil, P. Satapathy, S. P. Huheda, S. S. More, K. Muthucheliyan, T. N. Kumar, A. V. Raghu, K. R. Reddy, F. Zameer, *FlatChem.* **2020**. *23*, 100184.
[14] S. J. Malode, S. Pandiaraj, A. Alodhayb, N. P. Shetti, *ACS Appl. Bio Mater.* **2024**, *7*, 752–777.
[15] O. C. Compton, S. T. Nguyen, *Small* **2010**, *6*, 711–723.
[16] S. Saroj, P. Us, S. Patil, D. Paul, S. Saha, A. Ali, T. Rakshit, *ACS Appl. Bio Mater.* **2024**, *7*, 2741–2751.

[17] K. Yang, L. Feng, X. Shi, Z. Liu, *Chem. Soc. Rev.* **2013**, *42*, 530–547.
[18] R. Yanikoglu, C. Y. Karakas, F. Ciftci, M. A. Insel, Z. Karavelioglu, R. Varol, A. Yilmaz, R. Cakir, H. Uvet, C. B. Ustundag, *Pharmaceutics* **2024**, *16*, 837.
[19] A. Pourjavadi, S. Asgari, S. H. Hosseini, *J. Drug Deliv. Sci. Technol.* **2020**, *56*, 101542.
[20] A. M. Alqarni, M. P. Zeidler, *Biochem. Soc. Trans.* **2020**, *48*, 559–567.
[21] K. M. Hamed, I. M. Dighriri, A. F. Baomar, B. T. Alharthy, F. E. Alenazi, G. H. Alali, R. H. Alenazy, N. T. Alhumaidi, D. H. Alhulayfi, Y. B. Alotaibi, S. S. Alhumaidan, Z. A. Alhaddad, A. A. Humadi, S. A. Alzahrani, R. H. Alobaid, *Cureus* **2022**, *14*, e29518.
[22] A. Dehshahri, A. Kumar, V. S. Madamsetty, I. Uzieliene, S. Tavakol, F. Azedi, H. S. Fekri, A. Zarrabi, R. Muhammedinejad, V. K. Thakur, *Gels* **2020**, *7*, 2.
[23] S. Kumar, N. K. Garg, A. Jain, A. Khopade, P. Pandey, K. K. Sawant, *J. Drug Deliv. Technol.* **2023**, *88*, 104969.
[24] M. Mukhtar, A. L. Ezra Manicum, M. Shojaei Barjouei, R. Eshaghi Malekshah, R. Behzadmehr, A. Rahdar, S. Ghotekar, F. Baino, *Front. Biomater. Sci.* **2023**, *2*, 1200670.
[25] A. E. Alrefaei, M. A. Alzahrani, S. A. Alsuhaim, *Int. J. Med. Dev. Ctries.* **2022**, *6*, 740–747.
[26] B. T. Huang, Y. Tan, W. H. Zhao, Q. C. Zeng, B. S. Li, R. L. Chen, *J. Cancer Res. Clin. Oncol.* **2014**, *140*, 303–309.
[27] M. E. Burkard, K. B. Wisinski, U. O. Njiaju, S. Donohue, R. Hegeman, A. Stella, P. Mansky, V. Shah, T. Goggins, R. Qamar, L. Dietrich, K. Kim, A. M. Traynor, A. J. Tevaarwerk, *Clin. Breast Cancer* **2014**, *14*, 205–211.
[28] L. M. H. D. Mota, B. A. Cruz, C. V. Brenol, I. A. Pereira, L. S. Rezende-Fronza, M. B. Bertolo, M. V. C. D. Freitas, N. A. D. Silva, P. Louzada-Júnior, R. D. N. Giorgi, R. A. C. Lima, G. D. R. C. Pinheiro, *Rev. Bras. Reumatol.* **2012**, *52*, 152–174.
[29] E. M. Munyangango, C. Le Roux-Villet, S. Doan, F. Pascal, I. Soued, M. Alexandre, M. Heller, N. Lièvre, F. Aucouturier, F. Caux, C. Laroche, *Br. J. Dermatol.* **2013**, *168*, 381–390.
[30] S. R. Subramaniam, R. A. Cader, R. Mohd, K. W. Yen, H. A. Ghafor, *Am. J. Case Rep.* **2013**, *14*, 345–349.
[31] H. Sahrayi, E. Hosseini, S. Karimifard, N. Khayam, S. M. Meybodi, S. Amiri, M. Bourbour, B. F. Far, I. Akbarzadeh, M. Bhia, C. Hoskins, C. Chaiyasut, *Pharmaceuticals* **2021**, *15*, 6.
[32] Z. Shariatinia, N. Pourzadi, *J. Mol. Struct.* **2021**, *1242*, 130754.
[33] S. Ismail, S. Eljazzar, V. Ganji, *Foods* **2023**, *12*, 1612.
[34] P. Chanphai, T. J. Thomas, H. A. Tajmir-Riahi, *J. Biomol. Struct. Dyn.* **2021**, *39*, 787–794.
[35] M. Jurczyk, K. Jelonek, M. Musiał-kulik, A. Beberok, D. Wrze´sniok, J. Kasperczyk, *Pharmaceutics* **2021**, *13*, 326.
[36] X. Zhao, H. Li, R. J. Lee, *Expert Opin. Drug Deliv.* **2008**, *5*, 309–319.
[37] H. N. Abdelhamid, K. H. Hussein, *Biointerface Res. Appl. Chem.* **2021**, *11*, 14726–14735.
[38] W. S. Hummers Jr, R. E. Offeman, *J. Am. Chem. Soc.* **1958**, *80*, 1339–1339.
[39] P. Huang, C. Xu, J. Lin, C. Wang, X. Wang, C. Zhang, X. Zhou, S. Guo, D. Cui, *Theranostics* **2011**, *1*, 240–250.
[40] S. Sapino, S. Oliaro-Bosso, D. Zonari, A. Zattoni, E. Ugazio, *Int. J. Pharm.* **2017**, *530*, 239–248.
[41] F. Yang, N. Kamiya, M. Goto, *Eur. J. Pharm. Biopharm.* **2012**, *82*, 158–163.
[42] K. Kapoor, V. Pandit, U. Nagaich, *Int. J. Appl. Pharm.* **2020**, *12*, 33–39.
[43] H. X. Nguyen, A. K. Banga, *Pharm. Res.* **2018**, *35*, 1–20.
[44] S. Dash, P. N. Murthy, L. Nath, P. Chowdhury, *Acta Pol. Pharm.* **2010**, *67*, 217–223.
[45] P. Prajapati, M. Patel, Y. Kansara, P. Shah, V. S. Pulusu, S. Shah, *Sustain. Chem. Pharm.* **2024**, *39*, 101523.
[46] M. A. Insel, S. Karaku¸s, G. Temelcan, H. G. Kocken, I. Albayrak, *Phys. Scr.* **2023**, *98*, 035001.
[47] H. Akoglu, *Turk. J. Emerg. Med.* **2018**, *18*, 91–93.
[48] T. Bedir, D. Baykara, R. Yildirim, A. C. Calikoglu Koyuncu, A. Sahin, E. Kaya, G. Bosgelmez Tinaz, M. A. Insel, M. Topuzogulları, O. Gunduz, C. B. Ustundag, *Nanomaterials* **2024**, *14*, 563.
[49] R. Varol, Z. Karavelioglu, S. Omeroglu, G. Aydemir, A. Karadag, H. E. Meco, A. A. Demircali, A. Yilmaz, G. C. Kocal, G. Gencoglan, M. E. Oruc, G. B. Esmer, Y. Basbinar, S. K. Ozdemir, H. Uvet, *Nat. Commun.* **2022**, *13*, 7351.
[50] J. D. Clogston, A. K. Patri, *Characterization of Nanoparticles Intended for Drug Delivery*, Humana, New York, NY **2011**, pp. 63–70.
[51] M. R. Rajeev, V. Manjusha, T. S. Anirudhan, *J. Chem. Eng.* **2023**, *466*, 143244.
[52] A. Pourjavadi, S. Asgari, S. H. Hosseini, *J. Drug Deliv. Sci. Technol.* **2020**, *56*, 101542.
[53] K. Li, W. Zhong, P. Li, J. Ren, K. Jiang, W. Wu, *Int. J. Biol. Macromol.* **2023**, *252*, 126281.
[54] R. P. Jaya, in *New Materials in Civil Engineering*, Butterworth-Heinemann, **2020**, pp. 493–527.
[55] B. Lavakusa, B. S. Mohan, P. D. Prasad, N. Belachew, K. Basavaiah, *Int. J. Adv. Res.* **2017**, *5*, 405–412.
[56] N. Arjun, K. Uma, G. T. Pan, T. C. Yang, G. Sharmila, *Clean Technol. Environ. Policy* **2018**, *20*, 2025–035.
[57] R. Chuah, S. C. Gopinath, P. Anbu, M. N. Salimi, A. R. W. Yaakub, T. Lakshmipriya, *3 Biotech.* **2020**, *10*, 1–10.
[58] S. Veeresh, H. Ganesh, Y. S. Nagaraju, M. Vandana, S. P. Ashokkumar, L. Yesappa, H. Devendrappa, Structure, morphology and optical properties of graphene oxide In AIP Conference Proceedings, AIP Publishing, Mangalore, India **2020**, 2244.
[59] C. Y. Karakas, C. B. Ustundag, A. Sahin, J. Karadag, *Appl. Polym. Sci.* **2023**, *140*, e54683.
[60] N. Rahmanian, M. Eskandani, J. Barar, Y. Omidi, *J. Drug Targeting* **2017**, *25*, 202–215.
[61] I. Tufano, R. Vecchione, P. A. Netti, *Front. Bioengineer. Biotechnol.* **2020**, *8*, 613280.
[62] C. Tan, X. Cao, X. J. Wu, Q. He, J. Yang, X. Zhang, H. Zhang, *Chem. Rev.* **2017**, *117*, 6225–6331.
[63] S. Salatin, S. Maleki Dizaj, A. Yari Khosroushahi, *Cell Biol. Int.* **2015**, *39*, 881–890.
[64] V. C. Sanchez, A. Jachak, R. H. Hurt, A. B. Kane, *Chem. Res. Toxicol.* **2012**, *25*, 15–34.
[65] H. Yue, W. Wei, Z. Yue, B. Wang, N. Luo, Y. Gao, G. Ma, *Biomaterials* **2012**, *33*, 4013–4021.
[66] R. G. Mendes, A. Bachmatiuk, B. Büchner, G. Cuniberti, M. H. Rümmeli, *J. Mater. Chem. B* **2013**, *1*, 401–428.
[67] S. Sheikh, N. Goudarzian, *J. Univ. Chem. Technol. Metallurgy.* **2023**, *58*, 1019–1027.
[68] D. Bajas, G. Vlase, M. Mateescu, O. A. Grad, M. Bunoiu, T. Vlase, C. Avram, *Polymers* **2021**, *13*, 1–18.
[69] A. Fuliaş, C. Popoiu, G. Vlase, T. Vlase, D. Oneţiu, G. Săvoiu, G. Simu, C. Patruescu, G. Ilia, I. Ledeţi, *Dig. J. Nanomater. Biostruct.* **2014**, *9*, 93–98.
[70] L. Luo, T. Peng, M. Yuan, H. Sun, S. Dai, L. Wang, *Sensors* **2018**, *18*, 3745.
[71] S. Iqbal, S. Kainat, F. Jabeen, M. S. Sajid, S. Majeed, M. Najam-ul-Haq, *Sens. Bio-Sens. Res.* **2025**, *48*, 100807.
[72] J. Gul, A. Jabbar, S. Perveen, A. N. Awan, M. R. Shah, *J. Cluster Sci.* **2025**, *36*, 1–22.
[73] Y. J. Liou, W. J. Huang, *JMST* **2014**, *30*, 1088–1091.
[74] Y. Hong, Z. Wang, X. Jin, *Sci. Rep.* **2013**, *3*, 1–6.
[75] K. V. Pavan, M. Arthanareeswari, A. Ravikiran, P. Kamaraj, *Chem. Sci. Trans.* **2013**, *2(S1)*, S135-S140.
[76] X. Li, H. Wang, X. Zou, H. Su, C. Li, *Eur. J. Pharm. Sci.* **2022**, *170*, 106101.
[77] F. Ciftci, *Int. J. Biol. Macromol.* **2023**, *235*, 123769.
[78] A. Pourjavadi, S. Asgari, S. H. Hosseini, *J. Drug Deliv. Technol.* **2020**, *56*, 101542.
[79] T. Higuchi, *J. Pharm. Sci.* **1963**, *52*, 1145–1149.
[80] J. Siepmann, N. A. Peppas, *Adv. Drug Delivery Rev.* **2001**, *48*, 328–343.
[81] P. L. Ritger, N. A. Peppas, *J. Controlled Release* **1987**, *5*, 23–36.
[82] P. Costa, J. M. Sousa Lobo, *Eur. J. Pharm. Sci.* **2001**, *13*, 123–133.
[83] M. Raudenska, M. Kratochvilova, T. Vicar, J. Gumulec, J. Balvan, H. Polanska, J. Pribyl, M. Masarik, *Sci. Rep.* **2019**, *9*, 1660.
[84] L. D. Osborne, G. Z. Li, T. How, E. T. O'Brien, G. C. Blobe, R. Superfine, K. Mythreye, *MBoC* **2014**, *25*, 3528–3540.
[85] K. Fraczkowska, M. Bacia, M. Przybyło, D. Drabik, A. Kaczorowska, J. Rybka, E. Stefanko, S. Drobczynski, J. Masajada, H. Podbielska, T. Wrobel, M. Kopaczynska, *Biomed. Pharmacother.* **2018**, *97*, 1195–1203.
[86] M. Li, L. Liu, X. Xiao, N. Xi, Y. Wang, *J. Biol. Phys.* **2016**, *42*, 551–569.
[87] H. Zeng, C. Xia, B. Zhao, M. Zhu, H. Zhang, D. Zhang, X. Rui, H. Li, Y. Yuan, *Front. Pharmacol.* **2022**, *12*, 747992.
[88] S. J. Kim, C. X. Zhang, R. Demsky, S. Armel, Y. I. Kim, S. A. Narod, J. Kotsopoulos, *Breast Cancer Res. Treat.* **2019**, *174*, 741–748.
[89] B. Dutta; K. C. Barick; P. A. Hassan, *Adv. Colloid Interface Sci.* **2021**, *296*, 102509.

[90] K. Watanabe; M. Kaneko; Y. Maitani, *Int. J. Nanomed.* **2012**, *7*, 3679–3688.
[91] S. H. Kim; J. H. Jeong; K. W. Chun; T. G. Park, *Langmuir* **2005**, *21*, 8852–8857.
[92] J. Pan, K. Rostamizadeh, N. Filipczak, V. P. Torchilin, *Molecules* **2019**, *24*, 1035.
[93] P. Kulkarni, D. Rawtani, *J. Pharm. Sci.* **2019**, *108*, 2643–2653.
[94] L. Zhang, J. Xia, Q. Zhao, L. Liu, Z. Zhang, *Small* **2010**, *6*, 537–544.
[95] J. Rejman, V. Oberle, I. S. Zuhorn, D. Hoekstra, *Biochem. J.* **2004**, *377*, 159–169.
[96] I. Canton, G. Battaglia, *Chem. Soc. Rev.* **2012**, *41* 2718.
[97] A. Albanese, P. S. Tang, W. C. W. Chan, *Annu. Rev. Biomed. Eng.* **2012**, *14*, 1–16.

Manuscript received: January 23, 2025